Combined NMR, DFT and X-ray studies highlight structural and hydration changes of [Ln(AAZTA)]- complexes across the series

Combined NMR, DFT and X-ray studies highlight structural and hydration changes of [Ln(AAZTA)]− complexes across the series

Zsolt Baranyai, a Daniela Delli Castelli,b Carlos Platas-Iglesias,c David Esteban-Gomez, c Attila Bényei, d Lorenzo Tei, e and Mauro Botta, e

a Bracco Research Center, Bracco Imaging SpA, Via Ribes 5, Colleretto Giacosa (TO), 10010, Italy

b Department of Molecular Biotechnology and Health Science, University of Turin, Via Nizza 52, Torino, 10126, Italy

c Centro de Investigacions Cientificas Avanzadas (CICA) and Departamento de Quimica, Facultade de Ciencias, Universidade da Corunã, Corunã, 15071 A, Spain

d Department of Physical Chemistry, Faculty of Science and Technology, University of Debrecen, Egyetem tér 1, Debrecen, H-4032, Hungary

Abstract

We report a detailed structural study of [Ln(AAZTA)]- complexes by using a combination of experimental and theoretical tools. The analysis of the 1H NMR paramagnetic shift of the methyl peak across the series suggests that a structural change occurs between Ho and Er. Chemical exchange saturation transfer experiments were subsequently used to determine the number of coordinated water molecules and their corresponding exchange rates kex at 278 K. The Z-spectra recorded for the Ho(iii) complex present two signals that confirm the presence of two coordinated water molecules, which are endowed with rather different exchange rates: 5.8(±3.0) × 103 and 8.1(±0.5) × 104 s-1. On the contrary, the Er(iii) and Tm(iii) complexes present a single signal in the Z-spectra. The exchange rate of the coordinated water molecule(s) decreases markedly across the series from Gd(iii) to Yb(iii). DFT calculations support the change in hydration number by the end of the lanthanide series, which is the result of an increased steric compression around one of the coordinated water molecules on decreasing the size of the metal ion. X-ray diffraction studies on the Er(iii) complex confirm the presence of a single inner-sphere water molecule and the dodecahedral coordination environment of the metal ion.

Introduction

More than thirty years ago, Gd(iii) complexes were introduced as Magnetic Resonance Imaging (MRI) contrast agents (CAs) to improve the diagnostic potential of the technique. Since then, no other system has shown to possess the combination of those favourable

features necessary to replace such paramagnetic complexes in the clinical setting. However, as there is considerable scope for improvement in the clinically approved CAs, a large number of studies are nowadays in progress looking for optimized and more effective systems.1 Besides this established clinical role in diagnostic MR imaging, lanthanide(iii) complexes have been investigated for a number of biomedical applications, such as luminescent probes,2 Chemical Exchange Saturation Transfer (CEST) agents,3 chemical shift reagents4 and Magnetic Resonance Spectroscopy (MRS) agents.5 For their use as MRI probes, the Ln(iii) ion needs to be tightly coordinated by a multidentate organic ligand ensuring that at least one water molecule remains directly coordinated to the metal centre. As the coordination number of Ln(iii) ions ranges between 8 and 9, the chelator should be hepta- or octadentate to ensure the formation of complexes with high thermodynamic stability and pronounced kinetic inertness. The efficacy of these contrast agents depends on several physico-chemical parameters, among which the number (q) and the exchange rate (kex = 1/τM) of the coordinated water molecule(s) are of paramount importance.1 For instance, T1 agents' sensitivity is directly proportional to q and the optimal kex value should be in the range 107–109 s−1 to achieve optimal relaxation efficiency.1 On the contrary, for Ln(iii) complexes used as PARACEST agents the ideal kex value falls in the range is 102–104 s−1 and q only marginally affects the sensitivity.3 Many studies have been carried out to optimize these two parameters through rational changes of various features of the organic ligand structure while trying to preserve the stability of the complex.6 Recently, some of the paradigms established by previous investigations have been challenged by the behaviour shown by Ln(iii) complexes with AAZTA-like ligands (AAZTA = 6-amino-6-methylperhydro-1,4-diazepine tetraacetic acid, Scheme 1).7,8 For example, the assumption that anionic complexes are characterized by fast exchanging water molecules (kex ≥ 107 s−1)9 has been demonstrated of non-general validity in the case of [Yb(AAZTA)(H2O)]− and [Tm(AAZTA-Ph-NO2)(H2O)]− (Scheme 1). Moreover, the very slow kex of the complexes of these two ions as compared to [Gd(AAZTA)(H2O)2]− is in contrast to previous results that indicate an increase in kex values with the decrease of the ionic radius, both in the case of complexes with q = 1 and in that of complexes with q = 2.6 The only relevant exception is represented by the eight coordinate [Ln(PDTA)(H2O)2]− complexes (PDTA = propylenediamine-N,N,N',N'-tetraacetic acid) that exhibit a decrease of kex on proceeding across the Ln(iii) series, though not associated with a change in the hydration state.10

[Gd(AAZTA)(H2O)2]− and its derivatives are pseudo-macrocyclic complexes well recognized in the landscape of T1 agents as they show high relaxivity, mainly as a result of the presence of two water molecules in the inner coordination sphere of Gd(iii) in rapid exchange with the bulk water (kex = 1.1 × 107 s−1 at 298 K).11–13 This optimized efficiency has fostered the use of Gd(AAZTA)-like systems in in vivo preclinical MR-molecular imaging studies.14 Interestingly, a detailed study on the equilibrium and kinetic properties of Ln(AAZTA) complexes showed that AAZTA coordinates the lanthanide ions with log KML values in the range 17.5–21.8. Its affinity steadily increases from La(iii) to Lu(iii), with a significant rise of log KML for the last members of the series (in particular for Yb(iii) and Lu(iii)).15 This behaviour differs from that observed in case of Ln(iii) complexes with octadentate ligands like DTPA, DOTA or DOTA derivatives for which the stability constants of the chelates increase from La to Gd and then remain almost

constant for the heavier members of the series.16 The reason for this trend was ascribed to the flexibility of the ligand and to the more suitable size-match of the seven-membered diazepine skeleton to accommodate smaller metal ions.15

The equilibrium data on [Ln(AAZTA)]− complexes coupled to the observation that in case of [Yb(AAZTA)(H2O)]− and [Tm(AAZTA-Ph-NO2)(H2O)]− only one water molecule is coordinated to the metal centre, highlight that [Ln(AAZTA)]− complexes experience some structural change along the series causing the loss of one metal coordinated water molecule. Therefore, a systematic solution NMR study on [Ln(AAZTA)]− complexes is mandatory to analyse in detail the changes in their solution structure occurring along the series. In this work, we report the results of DFT analysis and X-ray crystallographic studies on [Er(AAZTA)(H2O)]− that support the high resolution NMR and CEST data and allow a more detailed understanding of the variation of kex along the series.

Results and discussion

Solution NMR studies

The 1H NMR spectra (9.4 and 14.1 T) of the [Ln(AAZTA)]− complexes (Ln = Nd, Eu, Tb, Dy, Ho, Er and Tm) were recorded in D2O at pH = 7.0 at different temperatures (278–310 K, Fig. S1–S7†). The spectra of the Nd, Eu, Dy, Tb and Yb8 chelates show nine signals distributed over a broad range of chemical shifts (eight with an identical peak area and the ninth with a relative intensity of 1.5), which points to an effective Cs symmetry of the complexes in solution. This implies the occurrence of a fluxional behaviour that averages the two acetate groups of the iminodiacetate moiety, the two acetate groups attached to the 1,4-diazepine and the methylene protons of the cycle. In the case of the Ho, Er and Tm complexes a lower number of signals is observed due to overlap with the residual solvent signal. Although little informative, the NMR proton spectra allow to easily identify the methyl peak that can be used to check the presence or absence of isostructurality along the lanthanides series. This can be done by analysing the LIS (Lanthanide Induced Shift) of a given peak of the complexes with the different Ln(iii) ions.17

The paramagnetic shifts observed in the 1H NMR spectra can be expressed as the sum of the contact (δc) and pseudocontact (δpc) contributions:

$$\delta^{para} = \delta^{obs} - \delta^{dia} = \delta^{c} + \delta^{pc} = \langle S_Z \rangle F + C_j D$$

The contact contribution is proportional to the reduced value of the average spin polarization 〈Sz〉, which was calculated for each lanthanide, and to the term F, which is proportional to the Fermi hyperfine coupling constant at the observed nucleus. The pseudocontact

contribution is proportional to the Bleaney constant Cj, which is characteristic of the Ln(iii) ion, and a constant D that contains a geometric factor and ligand field parameters. Thus, both the contact and pseudocontact contributions can be expressed as the product of a term characteristic of the lanthanide (〈Sz〉 and Cj) and a second term that is characteristic of the nucleus under study. Thus, eqn (1) can be conveniently rewritten in a linear form given by:17,18

$$\frac{\delta^{para}}{\langle S_z \rangle} = F + \frac{C_j}{\langle S_z \rangle} D.$$

The signal due to the methyl group of the ligand is easily identified by integration of the NMR peaks. The plot of the corresponding chemical shift values according to eqn (2) results in a linear trend for the lanthanide ions from Nd to Ho (R2 > 0.9979). However, the paramagnetic shifts of the three heaviest paramagnetic members of the lanthanide series (Er, Tm and Yb) fall out of the straight line (Fig. 1).

While this result should be taken with some care giving recent concerns on the validity of Bleaney's theory,19 it suggests that a structural change occurs across the lanthanide series with the changeover between Ho and Er, likely related to a change of the number of coordinated water molecules.

CEST studies

We have recently shown that [Yb(AAZTA)(H2O)]− features a single water molecule coordinated to the metal centre that exchanges very slowly with the bulk.8 The kex value determined (kex ∼ 6.5 × 103 s−1) represents an average between the value estimated by line shape analysis of the 1H NMR spectrum and that calculated by fitting the Z-spectrum to the Bloch equations. This value is also quite similar to that calculated for [Tm(AAZTA-Ph-NO2)]− from 1H NMR relaxometric data at 298 K.7

It is well established that Saturation Transfer (ST) is a useful NMR tool to identify exchanging peaks and measure their exchange rate. It consists in irradiating a signal of the spectrum with a selective RF pulse and observing the variations that this perturbation might induce on the other signals. If one or more of the other signals decrease the intensity, then a saturation

transfer has occurred and this unambiguously indicates that these two signals belong to protons in mutual exchange (provided that dipolar interaction and NOE effect can be excluded). Among others, the exchange rate between the two pools (kex) is one of the main parameters affecting the amount of saturation that can be transferred. The limit of this technique is that the experiment can be performed only when the exchanging pools are in slow exchange on the NMR timescale (Δω > kex).20 In the present study, we exploited ST to assess the presence in the [Ln(AAZTA)]− complexes of bound water molecules in slow exchange with the bulk. Owing to the very large LIS, the bound water molecules are expected to be under the slow exchange regime even for high values of kex (e.g. up to ∼1 × 105 s−1 for a peak at ±100 ppm). Very often mobile protons exchanging with bulk water with large kex values display signals characterized by a bandwidth too large to be detected directly in the NMR spectrum. For this reason, it is necessary to perform experiments by irradiating systematically and gradually all the frequencies over a sufficiently large range. The intensity of the bulk water signal is then plotted as a function of the irradiated offset to evidence the presence of very large exchanging peaks. These type of graphs are known as Z-spectra and are commonly used to describe and analyse saturation transfer phenomena. Z-spectra have been acquired at 600 MHz and 278 K for the AAZTA complexes of Ho, Er and Tm, at a concentration of 0.10 M (Fig. 2). The RF pulse power for the selective saturation was tuned to properly saturate the very large bound water resonance; in particular, a value of 100 μT was used for [Er(AAZTA)(H2O)]− and [Tm(AAZTA)(H2O)]−, whereas a power of 200 μT was needed to observe Saturation Transfer of [Ho(AAZTA)(H2O)2]− bound water molecules. In the Z-spectrum, the Tm and Er complexes display only one peak at 103 and 83.2 ppm, respectively. Previously published results showed the same pattern for [Yb(AAZTA)(H2O)]−. On the other hand, [Ho(AAZTA)(H2O)2]− displays two peaks at −47 ppm (peak A, Fig. 2) and −255 ppm (peak B, Fig. 2). These results can be explained on the hypothesis that [Ho(AAZTA)(H2O)2]− possesses two water molecules coordinated to the metal centre, whereas [Er(AAZTA)]− and [Tm(AAZTA)]− complexes are monohydrated (q = 1). We notice that the sign of the chemical shifts of coordinated water molecule(s) follows the qualitative trend predicted by Bleaney's theory,17 which provides positive Bleaney factors for Er(iii), Tm(iii) and Yb(iii), and negative for Ho(iii) (Table 1). The spectra were fitted to the Bloch equations and a rough estimate of the water exchange rate has been obtained: [Er(AAZTA)(H2O)]−: 8.7(±0.5) × 104 s−1; [Tm(AAZTA)(H2O)]−: 7.0(±0.5) × 104 s−1; [Ho(AAZTA)(H2O)2]−, peak A: 5.8(±3.0) × 103 s−1; peak B: 8.1(±0.5) × 104. These results highlight a rather unexpected and unprecedented decrease of the rate of water exchange by four order of magnitude on moving from [Gd(AAZTA)(H2O)2]− to [Yb(AAZTA)(H2O)]−. It is worth noting that the difference in kex is not only related to the change of q because a very slow kex was measured also for [Ho(AAZTA)(H2O)2]−. Interestingly, the ST technique allows determining independently the exchange rates of the two coordinated water molecules in [Ho(AAZTA)(H2O)2]−, while other techniques such as 17O NMR or 1H relaxometry generally provide weighted values of the individual exchange rates (i.e. for [Gd(AAZTA)(H2O)2]−). The kex values characterising the exchange rates of the two water molecules in the Ho(iii) complex differ by one order of magnitude, a fact that is likely related to the different strengths of the two Ho–Owater bonds (see below).

DFT calculations

In order to confirm the experimental NMR data, the relative stability of the mono- and bis-aquated forms of [Ln(AAZTA)]− complexes was investigated by using DFT calculations. We initially optimized the structures of the q = 2 complexes using the [Ln(AAZTA)(H2O)2]−·4H2O model systems, which include two explicit second sphere water molecules for each coordinated water molecule. Subsequently the structures of the q = 1 systems [Ln(AAZTA)(H2O)]−·5H2O were also optimized. The explicit inclusion of second-sphere water molecules together with a polarized continuum to account for bulk water effects was found to be critical to obtain accurate Ln–Owater distances and spin densities at the 17O nuclei.21 The optimized geometries present coordination environments that can be described as capped square antiprismatic and dodecahedral (Fig. 3). The relative free energies of the two species (Fig. 4) remain relatively constant in the first half of the lanthanide series, for which the bis-hydrated species is favoured by ∼30 kcal mol−1. The q = 1 species is progressively stabilized on proceeding across the second part of the lanthanide series, becoming the most stable form for the smallest Ln ions Tm, Yb and Lu. These results support a change in the hydration number close to the end of the lanthanide series, as suggested by the paramagnetic shifts and CEST analyses.

The analysis of the calculated Ln–Owater distances across the series gives some insight into the reasons for the rather abrupt stabilization of the q = 1 complex near the end of the lanthanide series (Fig. 5). The Ln–Owater distances calculated for the [Ln(AAZTA)(H2O)]−·5H2O systems decrease across the lanthanide series, as would be expected due to the lanthanide contraction. However, for the [Ln(AAZTA)(H2O)2]−·4H2O systems one of the Ln–Owater distances decreases steadily across the series, while the second one decreases from to La(iii) to Er(iii), and then becomes longer for the smallest Ln(iii) ions (Tm–Lu). This reflects an increasing steric hindrance around this water binding site, which results in a weaker binding of one of the coordinated water molecules in the bis-hydrated species, and thus in a stabilization of the monohydrated form for the smallest Ln(iii) ions.

The strength of the Ln–Owater interactions was assessed by calculating the electron densities at the concerned bond critical points (ρBCP). Previous studies showed that stronger Ln–Owater bonds are characterized by higher ρBCP values22 and thus lower water exchange rates.23 The Ln–Owater bonds of the [Ln(AAZTA)(H2O)2]−·4H2O and [Ln(AAZTA)(H2O)]−·5H2O systems are characterized by similar ρBCP values for the largest Ln(iii) ions, but they diverge as the size of the Ln(iii) ion decreases. The trend in ρBCP values calculated for the [Ln(AAZTA)(H2O)2]−·4H2O system parallels that of the distances, with the binding of one of the water molecules being dramatically weakened by the end of the series. The Ln–Owater bonds of the mono-hydrated species are characterized by high ρBCP values at the end of the series, which indicates a strong coordination of the water molecule.

X-ray structure of the [Er(AAZTA)(H2O)]− complex

Finally, we analysed the X-ray crystal structure of [Er(AAZTA)]− to find experimental evidence for the structural change observed across the Ln series and to confirm the presence of a single coordinated water molecule. In particular, single crystals of formula {(C(NH2)3)[Er(AAZTA)(H2O)]}·2H2O suitable for X-ray diffraction studies were grown from an aqueous solution. A simplified structure of the [Er(AAZTA)(H2O)]− complex and the selected bond distances are given in Fig. 6 and Table 2, respectively. Other 1H NMR spectra, crystallographic and computational details regarding the structure of [Er(AAZTA)(H2O)]− are reported in the ESI (Fig. S8 and S9 and Tables S1–S5†)

Three nitrogen and four carboxylate-oxygen donor atoms of the AAZTA ligand and one water molecule in the capping position provide the coordination polyhedron around Er(iii) in [Er(AAZTA)(H2O)]−. This can be best described by an irregular dodecahedron defined by a 1 : 4 : 3 stack (top to bottom in Fig. 6) of O1w (the water molecule) and of two nearly parallel planes (tilt angle of 7.90°): O11, O31, O33 and O41 (mean deviation from planarity 0.02 Å), and N1, N3 and N4 ones. The distance from the Er(iii) ion to the O11–O31–O33–O41 and N1–N3–N4 planes is 0.413 and 1.925 Å, respectively. The bond distances of Er(iii) with the coordinated N and O donor atoms of AAZTA ligand are in the expected ranges of 2.48–2.57 Å and 2.25–2.30 Å, with average values of 2.53 Å and 2.28 Å, respectively (Table 2).

The solid state structure of [Er(AAZTA)(H2O)]− is similar to the X-ray structure of [Sc(AAZTA)(H2O)]−,24 but differs from that of [Gd(AAZTA)(H2O)]−, characterized by a distorted bicapped square antiprismatic geometry (Table 2).25 The square planes of the antiprism in the [Gd(AAZTA)(H2O)]− complex are formed by three carboxylate and the water oxygen atoms (O4, O5, O2' and O1) and by the other by two nitrogen (N1 and N2) and two carboxylate oxygen atoms (O2 and O3), providing a twist angle between the two planes of 45°. The capping positions are occupied by one of the ring nitrogen atoms (N3) and an oxygen atom (O9') of a bridging carboxylate group of the neighbour [Gd(AAZTA)(H2O)]− entity. The Gd–OH2 distance (Gd–O1w: 2.443 Å) is about 0.095 Å longer than that of Er–OH2 (Er–O1w: 2.344 Å), which indicates the significantly stronger interaction of the smaller Er(iii) ion with the oxygen of the inner-sphere water molecule. The Er–OH2 distances obtained by X-ray diffraction studies (2.344 Å) and by DFT calculations (2.375 Å) are in very good agreement. On the other hand, the average Sc–N and Sc–O distances in the structurally analogue [Sc(AAZTA)(H2O)]− 24 complex are about 0.11 and 0.12 Å shorter than those of [Er(AAZTA)(H2O)]−. The smaller size and the similar charge result in the stronger interaction of the Sc(iii) ion with the inner sphere water molecule, which is clearly indicated by the 0.1 Å shorter Sc–OH2 distance compared with the Er–OH2 one.

Conclusions

The [Ln(AAZTA)]− complexes present a series of interesting properties for their applications as diagnostic imaging probes, which have made them the subject of various studies in the last ten years. Recently, it has been reported that the AAZTA complexes and one of its derivatives undergo a change in the state of hydration, from two to one, passing from Gd(iii) to Yb(iii), accompanied by a marked decrease in the rate of the water exchange process. The results obtained in this systematic study confirm the preliminary data and show that the kex values decrease with the decrease of the ionic radius following a trend that is not entirely predictable and in some aspects surprising. Furthermore, it has been shown that the marked decrease in the exchange rate along the series is the consequence of a structural change that takes place passing from [Ho(AAZTA)(H2O)2]− to [Tm(AAZTA)(H2O)]−. DFT calculations indicate that the complexes can adopt two stable geometries with different coordination polyhedra: a monocapped square antiprism (q = 2) and a dodecahedron (q = 1). The former is more stable for the complexes of the La–Ho cations while the second has a lower energy in the case of the complexes of the smaller ions (Er–Lu). The dodecahedron geometry, confirmed by X-ray diffraction studies on [Er(AAZTA)(H2O)]−, is rather unusual and it was not indicated by the thorough stereochemical analysis of the ideal eight-vertex polyhedra found for Ln(iii)-complexes (up to 11 different cases).26 Equilibria involving variously hydrated species also exist in the case of the Gd(iii) aqua ion, Gd(iii)-EDTA and Gd(iii)-CDTA systems, the eight-coordinate species being prevalent. However, it has been shown that the co-existence of two species in solution accelerates the kinetics of exchange of water molecules, as the population of the transition states along the reaction pathway is high and the energy of activation for the water exchange process is decreased.27 Conversely, our results show a pronounced decrease in exchange kinetics. Furthermore, in the case of [Ln(EDTA)]− chelates the transition from nine-coordinate to eight-coordinate species is very smooth,27 while in the case of the [Ln(AAZTA)]− complexes the change is rather sharp. This different behaviour is consistent with the different trend in the kex values.

Moreover, a very important aspect is that the change of structure along the series involves the shortening of the Ln–Ow distance for one inner sphere water molecule, due to the contraction of the ionic radius, while for the second water molecule the distance increases due to steric interactions. This result is in agreement with the presence, suggested by the analysis of the [Ho(AAZTA)(H2O)2]− CEST data, of two water molecules characterized by different rates of exchange. This result is interesting and relevant. The possibility that two (or more) water molecules coordinated to the same metal ion may have different rates of exchange has been suggested previously, based on the analysis of 1H and 17O NMR relaxation data related to the formation of ternary compounds with monodentate anions.28 More recently, we have observed a difference of more than three orders of magnitude in the kex values of two macrocyclic complexes that differ in the position of the water molecule: in a capping position in one isomer and in the upper square plane of the twisted square antiprism in the other isomer.29

The results reported here represent a significant advance in the rational design of Gd-based MRI probes with increased hydration number and in the development of stable and biocompatible CEST probes for in vivo MRI preclinical applications. In addition, the possibility to modulate in a differentiated manner the lability of water molecules coordinated to the same metal centre offers new perspectives for the control of their reactivity.

Experimental section

Chemicals and materials

All chemicals were purchased from Sigma-Aldrich Co. and used without further purification. [Ln(AAZTA)]− complexes were readily synthesized by adding a slight stoichiometric excess (5–10%) of $LnCl_3$ in aqueous solution to a solution of the AAZTA ligand (synthesized as reported in ref. 11) in water at room temperature. The pH was maintained around 7 by means of 0.1 M NaOH. The pH was then increased to nine to precipitate excess Ln(iii) as $Ln(OH)_3$. The solution was centrifuged (4000 rpm, 3 min, r.t.) and the supernatant filtered through a 0.2 μm filter. The pH was re-adjusted to 7 and the solvent removed in vacuo to obtain a colourless solid. This procedure ensures the absence of excess ligand or free metal ion in the final solution. In fact, the xylenol orange indicator verified the absence of free Ln(iii).

High resolution NMR spectra and saturation transfer measurements

[Ln(AAZTA)]− complexes were dissolved in D_2O, and the pD was adjusted to 7.4 (pH = 7.0) by addition of DCl or KOD and checked with a glass electrode connected to an AS instruments pH-meter. The spectra were recorded at 9.4 T and 14.1 T on Bruker DRX 400 and Avance 600 spectrometers, respectively. The temperature was controlled with Bruker thermostating units, and high resolution spectra have been acquired by varying the temperature from 278 K to 350 K. The saturation transfer experiments were carried out at 278 K by irradiating the sample dissolved in water with a 200 μT ([Ho(AAZTA)(H_2O)2]−) or 100 μT ([Tm(AAZTA)(H_2O)]−, [Er(AAZTA)(H_2O)]−) continuous wave presaturation pulse for 1s. The CEST effect was measured recording a Z-spectra that record the intensity of water signal as a function of the irradiation frequency using a fixed irradiation time and irradiation power. The measurements were carried out at 14.1 T on a Bruker Avance 600 spectrometer. To evaluate kex values, Z-spectra were fitted against Bloch equations.

Computational details

All calculations were performed employing DFT within the hybrid meta-GGA approximation with the M062X exchange–correlation functional,30 and the Gaussian 09 package (Revision E.01).31 Our calculations used a mixed cluster/continuum approach with the explicit inclusion of two inner- and four second-sphere water molecules for the [Ln(AAZTA)(H_2O)2]−·4H_2O systems (Ln = La–Lu, except Pm). Geometry optimizations were

performed with the quasi-relativistic large-core effective core potential (LCRECP) of Dolg et al. and the related (7s6p5d)/[5s4p3d]-GTO valence basis set for the lanthanides,32 and the standard 6-311G(d,p) basis set for the remaining atoms. Large-core pseudopotential calculations include the 4f electrons in the core, and thus they were conducted on a pseudo-singlet state configuration. The stationary points found on the potential energy surfaces were confirmed to correspond to energy minima rather than saddle points via frequency analysis. Bulk solvent effects were considered by using the integral equation formalism variant of the polarizable continuum model (IEFPCM),33 employing the universal force field radii (UFF)34 scaled by a factor of 1.1 to define the solute cavities. Wave function analysis was carried out with the computer program Multiwfn 3.2.,35 which allows computing the electron density (ρ) and its Laplacian (∇2ρ) at the bond critical points (BCPs). Molecular graphics were generated using USCF Chimera (version 1.8).36

X-ray diffraction studies

Single crystals of {(C(NH2)3)[Er(AAZTA)(H2O)]}·2H2O have been prepared by mixing equimolar solid Er(OH)3 and H4AAZTA in water. The pH was adjusted to 6 by guanidine-carbonate (CO2 was eliminated by boiling the aqueous solution). The crystals were very thin needles and gave a low intensity diffraction pattern. A crystal well-looking in polarized light was fixed on a Mitegen loop using high viscosity oil. Data were collected at 118 K using a Bruker-D8 Venture diffractometer equipped with INCOATEC IμS 3.0 dual (Cu and Mo) sealed tube microsources and Photon 200 Charge-integrating Pixel Array detector. MoKα (λ = 0.71073 Å) radiation was applied. Several datasets were collected and all measurements supported the given structure. Data collection and integration was performed using the APEX3 software.37 Data reduction and multi-scan absorption correction was applied. The structure could be easily solved using direct methods and refined on F2 using SHELXL program38 incorporated into the APEX3 suite. Refinement was performed anisotropically for all non-hydrogen atoms. Hydrogens were placed into geometric positions except water protons which could be found on the difference electron density map and their distances to the oxygen atom were constrained. Further details of structure determination are collected in ESI and in CCDC 1960608.†

Conflicts of interest

There are no conflicts to declare.

Acknowledgements

C. P.-I. and D. E.-G. thank Ministerio de Economía y Competitividad (CTQ2016-76756-P) and Xunta de Galicia (ED431B 2017/59 and ED431D 2017/01) for generous financial support and Centro de Supercomputación de Galicia (CESGA) for providing the computer facilities. The research was also supported by the EU and co-financed by the European Regional Development Fund under the projects GINOP-2.3.2-15-2016-00008 and GINOP-2.3.3-15-

2016-00004. L. T. and M. B. acknowledge the financial support from Università del Piemonte Orientale (Ricerca locale 2019). The work was carried out within the framework of the COST CA15209 Action ‘European Network on NMR Relaxometry’.

Notes and references

1 (a) J. Wahsner, E. M. Gale, A. Rodríguez-Rodríguez and

P. Caravan, Chemistry of MRI contrast agents: current challenges and new frontiers, Chem. Rev., 2019, 119, 957;

(b) A. E. Merbach, L. Helm and É. Tóth, The chemistry of

contrast agents in medical magnetic resonance imaging, John

Wiley & Sons, New York, 2nd edn, 2013; (c) L. Helm,

J. R. Morrow, C. J. Bond, F. Carniato, M. Botta, M. Braun,

Z. Baranyai, R. Pujales-Paradel, M. Regueiro-Figuero,

D. Esteban-Gómez, C. Platas-Iglesias and T. J. Scholl,

Contrast Agents for MRI: Experimental Methods, ed.

V. C. Pierre and M. J. Allen, The Royal Society of Chemistry,

2017, ch. 2, pp. 121–242.

2 S. Shuvaev, M. Starck and D. Parker, Responsive, watersoluble Europium(III) luminescent probes, Chem. Eur. J.,

2017, 23, 9974; S. H. Hewitt and S. J. Butler, Application of

lanthanide luminescence in probing enzyme activity,

Chem. Commun., 2018, 54, 6635.

3 E. Terreno, W. Dastru, D. Delli Castelli, E. Gianolio,

S. Geninatti Crich, D. Longo and S. Aime, Advances in

metal-based probes for MR molecular imaging applications, Curr. Med. Chem., 2010, 17, 3684.

4 S. Posse, R. Otazo, S. R. Dager and J. Alger, MR spectroscopic imaging: principles and recent advances, J. Magn.

Reson. Imaging, 2013, 37, 1301; K. L. Peterson, K. Srivastava

and V. C. Pierre, Fluorinated paramagnetic complexes: sensitive and responsive probes for Magnetic Resonance

Spectroscopy and Imaging, Front. Chem., 2018, 6, 160.

5 (a) M. Zaiss and P. Bachert, Chemical exchange saturation

transfer (CEST) and MR Z-spectroscopy in vivo: a review of

theoretical approaches and methods, Phys. Med. Biol.,

2013, 58, 221; (b) M. Woods, D. E. Woessner and

A. D. Sherry, Paramagnetic lanthanide complexes as

PARACEST agents for medical imaging, Chem. Soc. Rev.,

2006, 35, 500.

6 (a) B. N. Siriwardena-Mahanama and J. M. Allen, Strategies

for optimizing water-exchange rates of lanthanidebased contrast agents for Magnetic Resonance Imaging,

Molecules, 2013, 18, 9352; (b) P. Caravan, D. EstebanGómez, A. Rodríguez-Rodríguez and C. Platas-Iglesias,

Water exchange in lanthanide complexes for MRI applications. Lessons learned over the last 25 years, Dalton

Trans., 2019, 48, 11161.

7 S. Karimi, L. Tei, M. Botta and L. Helm, Evaluation of water

exchange kinetics on [Ln(AAZTAPh–NO2)(H2O)q]

x complexes using proton Nuclear Magnetic Resonance, Inorg.

Chem., 2016, 55, 6300.

8 D. Delli Castelli, L. Tei, F. Carniato, S. Aime and M. Botta,

[Yb(AAZTA)(H2O)]−: an unconventional ParaCEST MRI

probe, Chem. Commun., 2018, 54, 2004.

9 A. O. Olatunde, J. M. Cox, M. D. Daddario, J. A. Spernyak,

J. B. Benedict and J. R. Morrow, Seven-coordinate CoII, FeII

and six-coordinate NiII amide-appended macrocyclic complexes as ParaCEST agents in biological media, Inorg.

Chem., 2014, 53, 8311.

10 N. Graeppi, D. H. Powell, G. Laurenczy, L. Zekany and

A. E. Merbach, Coordination equilibria and water exchange

kinetics of lanthanide(III) propylenediamine tetraacetates

and other magnetic resonance imaging related complexes,

Inorg. Chim. Acta, 1995, 235, 311.

11 S. Aime, L. Calabi, C. Cavallotti, E. Gianolio,

G. B. Giovenzana, P. Losi, A. Maiocchi, G. Palmisano and

M. Sisti, [Gd-AAZTA]−: a new structural entry for an

improved generation of MRI contrast agents, Inorg. Chem.,

2004, 43, 7588.

12 (a) G. Gugliotta, M. Botta and L. Tei, AAZTA-based bifunctional chelating agents for the synthesis of multimeric/dendrimeric MRI contrast agents, Org. Biomol. Chem., 2010, 8,

4569; (b) G. Gugliotta, M. Botta, G. B. Giovenzana and

L. Tei, Fast and easy access to efficient bifunctional chelators for MRI applications, Bioorg. Med. Chem. Lett., 2009,

19, 3442.

13 A. Vagner, E. Gianolio, S. Aime, A. Maiocchi, I. Toth,

Z. Baranyai and L. Tei, High kinetic inertness of a bishydrated Gd-complex with a constrained AAZTA-like ligand,

Chem. Commun., 2016, 52, 11235.

14 D. L. Longo, F. Arena, L. Consolino, P. Minazzi, S. GeninattiCrich, G. B. Giovenzana and S. Aime, Gd-AAZTA-MADEC, an

improved blood pool agent for DCE-MRI studies on mice on

1 T scanners, Biomaterials, 2016, 75, 47.

15 Z. Baranyai, F. Uggeri, G. B. Giovenzana, A. Benyei,

E. Brucher and S. Aime, Equilibrium and kinetic properties

of the lanthanoids(III) and various divalent metal complexes of the heptadentate ligand AAZTA, Chem. – Eur. J.,

2009, 15, 1696.

16 (a) E. Brücher, G. Tircsó, Z. Baranyai, Z. Kovács and

A. D. Sherry, in The Chemistry of Contrast Agents in Medical

Magnetic Resonance Imaging, ed. A. S. Merbach, L. Helm

and E. Toth, John Wiley & Sons, Ltd, 2nd edn, 2013,

pp. 157–208; (b) L. Tei, Z. Baranyai, L. Gaino, A. Forgács,

A. Vágner and M. Botta, Thermodynamic stability, kinetic inertness and relaxometric properties of monoamide derivatives of lanthanide(III) DOTA complexes, Dalton Trans., 2015, 44, 5467.

17 J. A. Peters, J. Huskens and D. J. Raber, Lanthanide induced shifts and relaxation rate enhancements, Prog. Nucl. Magn. Reson. Spectrosc., 1996, 28, 283.

18 (a) C. N. Reilley, B. W. Good and R. D. Allendoerfer, Separation of contact and dipolar lanthanide induced nuclear magnetic resonance shifts: evaluation and application of some structure independent methods, Anal. Chem., 1976, 48, 1446; (b) E. Terazzi, J.-P. Rivera, N. Ouali and C. Piguet, A justification for using NMR model-free methods when investigating the solution structures of rhombic paramagnetic lanthanide complexes, Magn. Reson. Chem., 2006, 44, 539.

19 (a) A. M. Funk, K.-L. N. A. Finney, P. Harvey, A. M. Kenwright, E. R. Neil, N. J. Rogers, P. K. Senanayake and D. Parker, Critical analysis of the limitations of Bleaney's theory of magnetic anisotropy in paramagnetic lanthanide coordination complexes, Chem. Sci., 2015, 6, 1655–1662; (b) G. Castro, M. Regueiro-Figueroa, D. Esteban-Gomez, P. Perez-Lourido, C. Platas-Iglesias and L. Valencia, Magnetic Anisotropies in Rhombic Lanthanide(III) Complexes Do Not Conform to Bleaney's Theory, Inorg. Chem., 2016, 55, 3490–3497.

20 M. Zaiss, G. Angelovski, E. Demetriou, M. T. McMahon,

X. Golay and K. Scheffler, QUESP and QUEST revisited - fast and accurate quantitative CEST experiments, Magn. Reson. Med., 2018, 79, 1708–1721.

21 D. Esteban-Gómez, A. de Blas, T. Rodríguez-Blas, L. Helm and C. Platas-Iglesias, Hyperfine Coupling Constants on Inner-Sphere Water Molecules of GdIII-Based MRI Contrast Agents, ChemPhysChem, 2012, 13, 3640–3650.

22 J. Zhang and M. Dolg, Labile Capping Bonds in Lanthanide(III) Complexes: Shorter and Weaker, J. Phys. Chem. A, 2015, 119, 774–780.

23 (a) M. Regueiro-Figueroa and C. Platas-Iglesias, Toward the Prediction of Water Exchange Rates in Magnetic Resonance Imaging Contrast Agents: A Density Functional Theory Study, J. Phys. Chem. A, 2015, 119, 6436–6445; (b) S. Karimi, G. Hunter, L. Moriggi, C. Platas-Iglesias and L. Helm, Complexation of [Gd(DTTA–Me)(H2O)2] – by Fluoride and Its Consequences to Water Exchange, Inorg. Chem., 2016, 55, 6231–6239.

24 G. Nagy, D. Szikra, G. Trencsényi, A. Fekete, I. Garai, A. M. Giani, R. Negri, N. Masciocchi, A. Maiocchi, F. Uggeri, I. Tóth, S. Aime, G. B. Giovenzana and Z. Baranyai, AAZTA: An Ideal Chelating Agent for the Development of 44Sc PET Imaging Agents, Angew. Chem., Int. Ed., 2017, 56, 2118–2122.

25 S. Aime, G. Bombieri, C. Cavallotti, G. B. Giovenzana, D. Imperio and N. Marchini, An unusual gadolinium tencoordinated dimeric complex in the series of MRI contrast agents: Na[Gd(H2O)AAZTA]·3H2O, Inorg. Chim. Acta, 2008, 361, 1534–1541.

26 D. Casanova, M. Llunell, P. Alemany and S. Alvarez, The

rich stereochemistry of eight-vertex polyhedra: a continuous shape measures study, Chem. – Eur. J., 2005, 11, 1479–

1494.

27 R. Janicki and A. Mondry, Structural and thermodynamic

aspects of hydration of Gd(III) systems, Dalton Trans., 2019,

48, 3380–3391.

28 M. Botta, S. Aime, A. Barge, G. Bobba, R. S. Dickins,

D. parker and E. Terreno, Ternary complexes between cationic GdIII chelates and anionic metabolites in aqueous

solution: an NMR relaxometric study, Chem. – Eur. J., 2003,

9, 2102–2109.

29 A. Rodriguez-Rodriguez, M. Regueiro-Figueroa, D. EstebanGomez, T. Rodriguez-Blas, V. Patinec, R. Tripier, G. Tircso,

F. Carniato, M. Botta and C. Platas-Iglesias, Definition of

the labile capping bond effect in lanthanide complexes,

Chem. – Eur. J., 2017, 23, 1110–1117.

30 Y. Zhao and D. G. Truhlar, The M06 suite of density functionals for main group thermochemistry, thermochemical

kinetics, noncovalent interactions, excited states, and transition elements: two new functionals and systematic

testing of four M06-class functionals and 12 other functionals, Theor. Chem. Acc., 2007, 120, 215–241.

31 M. J. Frisch, G. W. Trucks, H. B. Schlegel, G. E. Scuseria,

M. A. Robb, J. R. Cheeseman, G. Scalmani, V. Barone,

B. Mennucci, G. A. Petersson, H. Nakatsuji, M. Caricato,

X. Li, H. P. Hratchian, A. F. Izmaylov, J. Bloino, G. Zheng,

J. L. Sonnenberg, M. Hada, M. Ehara, K. Toyota, R. Fukuda,

J. Hasegawa, M. Ishida, T. Nakajima, Y. Honda, O. Kitao,

H. Nakai, T. Vreven, J. A. Montgomery, Jr., J. E. Peralta,

F. Ogliaro, M. Bearpark, J. J. Heyd, E. Brothers,

K. N. Kudin, V. N. Staroverov, R. Kobayashi, J. Normand,

K. Raghavachari, A. Rendell, J. C. Burant, S. S. Iyengar,

J. Tomasi, M. Cossi, N. Rega, J. M. Millam, M. Klene,

J. E. Knox, J. B. Cross, V. Bakken, C. Adamo, J. Jaramillo,

R. Gomperts, R. E. Stratmann, O. Yazyev, A. J. Austin,

R. Cammi, C. Pomelli, J. W. Ochterski, R. L. Martin,

K. Morokuma, V. G. Zakrzewski, G. A. Voth, P. Salvador,

J. J. Dannenberg, S. Dapprich, A. D. Daniels, Ö. Farkas,

J. B. Foresman, J. V. Ortiz, J. Cioslowski and D. J. Fox,

Gaussian 09, Revision E.01, Gaussian, Inc., Wallingford CT,

2009.

32 M. Dolg, H. Stoll, A. Savin and H. Preuss, Energy-adjusted

pseudopotentials for the rare earth elements, Theor. Chim.

Acta, 1989, 75, 173–194.

33 J. Tomasi, B. Mennucci and R. Cammi, Quantum mechanical continuum solvation models, Chem. Rev., 2005, 105,

2999–3093.

34 A. K. Rappe, C. J. Casewit, K. S. Colwell, W. A. Goddard III

and W. M. Skiff, UFF, a full periodic table force field for

molecular mechanics and molecular dynamics simulations, J. Am. Chem. Soc., 1992, 114, 10024–10035.

35 T. Lu and F. Chen, Multiwfn: A multifunctional wavefunction analyzer, J. Comput. Chem., 2012, 33, 580–592.

36 E. F. Pettersen, T. D. Goddard, C. C. Huang, G. S. Couch,

D. M. Greenblatt, E. C. Meng and T. E. Ferrin, UCSF

Chimera–a visualization system for exploratory research

and analysis, J. Comput. Chem., 2004, 25, 1605–1612.

37 Bruker, APEX3 (version: 6.2.6), SAINT (version: 8.38A),

SADABS (version: 2016/2), Bruker AXS Inc., Madison,

Wisconsin, USA, 2017.

38 SHELXL, version 2016/4; G. M. Sheldrick, Crystal structure

refinement with SHELXL, Acta Crystallogr., Sect. C: Struct.

Chem., 2015, 71, 3–8.

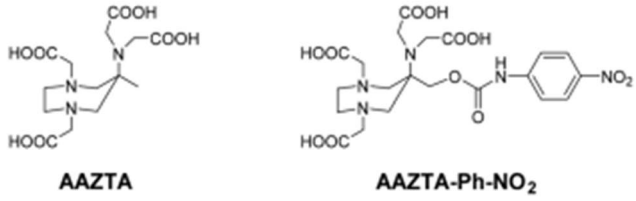

Scheme 1 Chemical structures of AAZTA and AAZTA-Ph-NO_2.

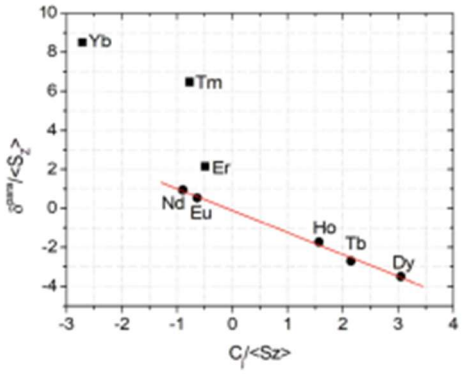

Fig. 1 Plot of the observed paramagnetic shifts for the methyl protons of $[Ln(AAZTA)]^-$ complexes.

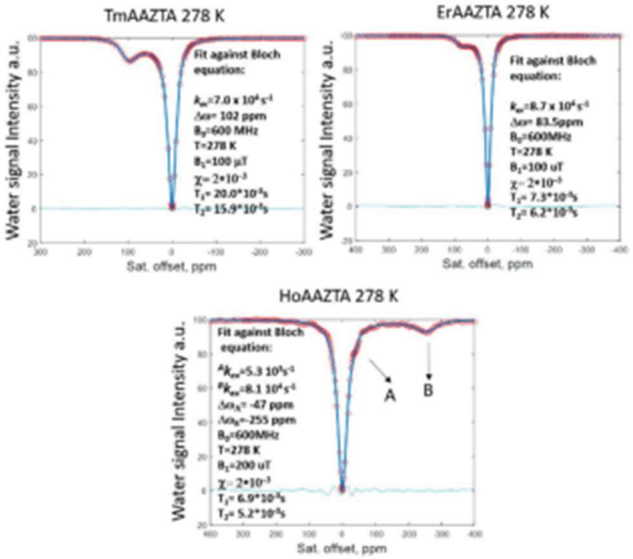

Fig. 2 Z-spectra recorded from 0.1 M solutions of AAZTA complexes in H_2O (278 K, 600 MHz). The solid lines correspond to the fit of the data to the Bloch equations.

Table 1 Chemical shifts (ppm) and exchange rates (s^{-1}, 278 K) of coordinated water molecules in [Ln(AAZTA)]$^-$ complexes

	δ/ppm	k_{ex}/s^{-1}
Gd[a]	—	1.1×10^6
Ho	−47	$5.8(\pm3.0) \times 10^3$
	−255	$8.1(\pm0.5) \times 10^4$
Er	83.2	$8.7(\pm0.5) \times 10^4$
Tm	103	$7.0(\pm0.5) \times 10^4$
Yb[b]	83	6.67×10^3

[a] Data obtained using ^{17}O NMR measurements from ref. 11. [b] From ref. 8.

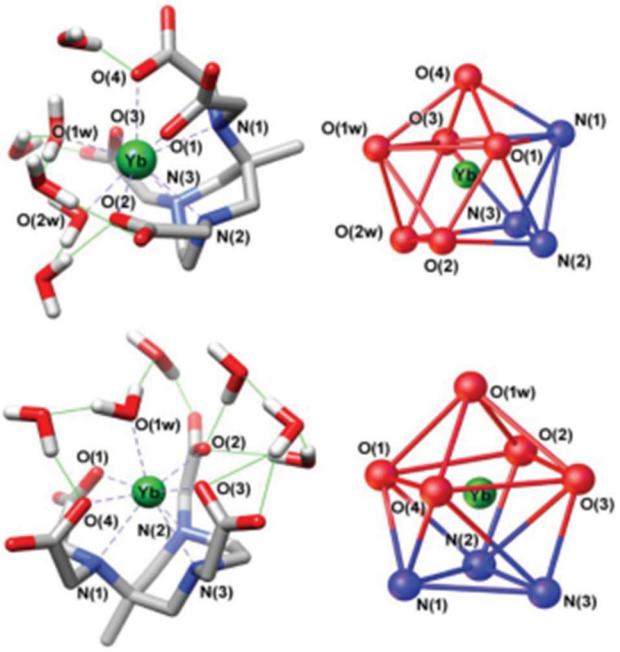

Fig. 3 Optimised geometries of the [Ln(AAZTA)$(H_2O)_2$]$^-$·4H_2O (top) and [Ln(AAZTA)(H_2O)]$^-$·5H_2O (bottom) systems.

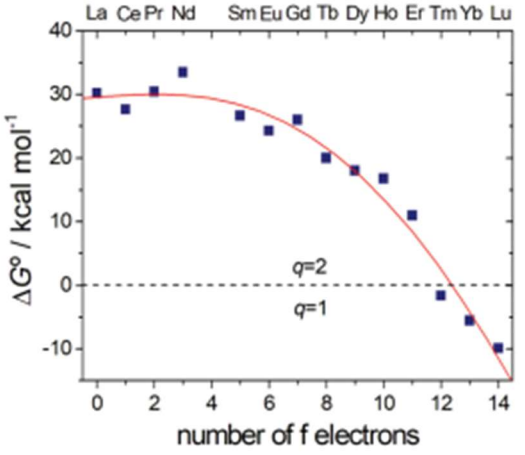

Fig. 4 Relative free energies of the $[Ln(AAZTA)(H_2O)_2]\cdot 4H_2O$ and $[Ln(AAZTA)(H_2O)]\cdot 5H_2O$ systems obtained with DFT calculations.

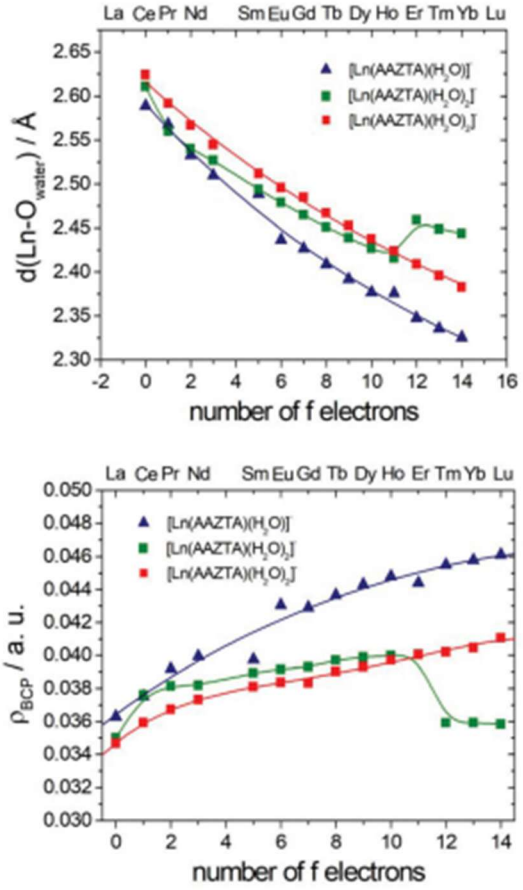

Fig. 5 $Ln-O_{water}$ bond distances (top) and electron densities at the corresponding bond critical points (bottom) calculated for the $[Ln(AAZTA)(H_2O)_2]\cdot 4H_2O$ (squares) and $[Ln(AAZTA)(H_2O)]\cdot 5H_2O$ (triangles) systems with DFT calculations. The solid lines are simply a guide for the eye.

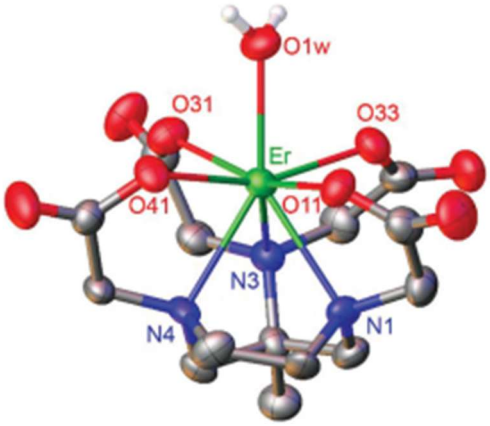

Fig. 6 View of the $[Er(AAZTA)(H_2O)]^-$ ion present in the single crystal of $((C(NH_2)_3)[Er(AAZTA)(H_2O)])\cdot 2H_2O$. Hydrogen atoms are omitted for simplicity. Color code: Er (green), O (red), N (blue) and C (grey).

Table 2 Selected bond angles (°) and distances in $[Er(AAZTA)(H_2O)]^-$, $[Gd(AAZTA)(H_2O)]^-$ and $[Sc(AAZTA)(H_2O)]^-$ complexes[24,25]

	Er(III)		Gd(III)[25]		Sc(III)[24]
Er–N1	2.468(9)	Gd–N1	2.599	Sc–N1	2.412
Er–N3	2.57 (1)	Gd–N2	2.681	Sc–N2	2.443
Er–N4	2.553 (9)	Gd–N3	2.778(5)	Sc–N3	2.476
Er–O11	2.302 (8)	Gd–O2	2.526(4)	Sc–O1	2.202
Er–O31	2.300 (8)	Gd–O3	2.402(4)	Sc–O3	2.152
Er–O33	2.247 (8)	Gd–O4	2.399(4)	Sc–O5	2.119
Er–O41	2.290 (8)	Gd–O5	2.442(4)	Sc–O7	2.158
Er–$O1_W$	2.344 (9)	Gd–O2′	2.548(4)	Sc–$O5_W$	2.247
		Gd–O9′	2.665(4)		
		Gd–$O1_w$	2.443(5)		
Geometry	Dodecahedron	Square antiprism		Dodecahedron	
O_4–N_3 tilt (°)	7.90	O_4-(N_2O_2) twist (°)	45	O_4–N_3 tilt (°)	8.35